AGU PUBLICATIONS

JGR

Journal of Geophysical Research: Earth Surface

RESEARCH ARTICLE

10.1002/2015JF003660

Topographically mediated ice stream subglacial drainage networks

J. Hiester[1], O. V. Sergienko[2], and C. L. Hulbe[3]

[1]Institute for Geophysics Jackson School of Geosciences, University of Texas at Austin, Austin, Texas, USA, [2]GFDL/AOS Princeton University, Princeton, New Jersey, USA, [3]School of Surveying, University of Otago, Dunedin, New Zealand

Key Points:
- Bed topography determines morphology of subglacial drainage system
- The coupled ice stream/subglacial water system evolves on short timescales
- Coupling between ice stream and subglacial water flow results in high effective stresses in ice

Supporting Information:
- Text S1
- Movie S1
- Movie S2
- Movie S3
- Movie S4
- Movie S5
- Movie S6
- Movie S7

Correspondence to:
O. V. Sergienko,
osergien@princeton.edu

Citation:
Hiester, J., O. V. Sergienko, and C. L. Hulbe (2016), Topographically mediated ice stream subglacial drainage networks, *J. Geophys. Res. Earth Surf.*, *121*, 497–510, doi:10.1002/2015JF003660.

Received 2 JUL 2015
Accepted 4 FEB 2016
Accepted article online 6 FEB 2016
Published online 29 FEB 2016

Abstract Satellite laser altimetry reveals short timescale changes in Antarctic ice sheet surface elevation that are suggested to be driven by subglacial water transport and storage. Here details of the interaction between the dynamics of ice stream flow, subglacial water system, and bed elevation relief are examined in the context of idealized, heterogeneous bed geometries. Using a two-way coupled model of ice and subglacial water flow, we show that basal topography controls the temporal and spatial variability of the sub–ice stream hydraulic system. The orientation and characteristic dimensions of the topographic undulations determine the morphology (connected subglacial ponds or channel-like subglacial water features) and timescales of the sub–ice stream drainage system. The short-term (several years to decades) variability of the simulated coupled ice stream/subglacial water system suggests that the short-term surface variations detected in remote sensing observations may be indicative of a rapidly evolving subglacial water system. Our simulations also show that interaction between ice flow and the highly dynamic subglacial water system has a strong effect on effective stress in the ice. Large effective stress magnitudes arise over areas where the basal traction is characterized by strong spatial gradients, that is, transitions from high to low basal traction or vise versa. These transitions migrate on multiyear timescales and thus cause large effective stress variability on the same temporal scales.

1. Introduction

Short timescale—1 to 3 years—changes in ice surface elevation have been interpreted as representing the movement and storage of subglacial water under Antarctic ice sheets [*Gray et al.*, 2005; *Fricker et al.*, 2007; *Carter et al.*, 2011]. These observations have been used in Antarctica to map the locations of and track changes in ponded subglacial water [*Gray et al.*, 2005; *Wingham et al.*, 2006; *Fricker et al.*, 2007; *Fricker and Scambos*, 2009; *Smith et al.*, 2009]. The subglacial hydrologic networks investigated in this way are extensive—connecting "lakes" up to 290 km apart—and capable of rapid, large-volume discharge events [*Wingham et al.*, 2006; *Carter et al.*, 2009]. Subglacial lakes have been detected along the length of some ice streams, from their catchments to their grounding lines, and as a component of the subglacial hydrologic system must be intimately associated with fast ice flow [*Siegert and Bamber*, 2000; *Fricker et al.*, 2007; *Tulaczyk et al.*, 2008].

Subglacial lakes have been identified and classified in terms of their signatures in ice-penetrating radar [*Carter et al.*, 2007, 2011] and their temporal attributes observed in repeat track ICESat laser altimeter measurements [e.g., *Smith et al.*, 2009]. Lake location tends to follow the shapes of the ice surface and the subglacial bed, and apparent transfer of water along lake networks appears to be related to topographic setting as well [*Wingham et al.*, 2006]. That context likely affects the role that subglacial lakes and lake networks play in ice stream variability [*Fried et al.*, 2014]. As ice stream flow is gravity driven, the surface undulations reflect the effects of basal conditions (topography and traction) on ice flow [e.g., *Schoof*, 2002; *Gudmundsson*, 2003; *Sergienko*, 2012, 2013]. It is thus of interest to investigate how bed shape influences basal water system development so that both remote sensing observations and ice stream change over time may be better understood.

In order to focus on the effects of the coupling between the ice and subglacial water flows, as well as their response to the effects of basal topography, we use the simplest possible formulations of a subglacial hydraulic system and ice stream that adequately simulates their response to varied basal topographies.

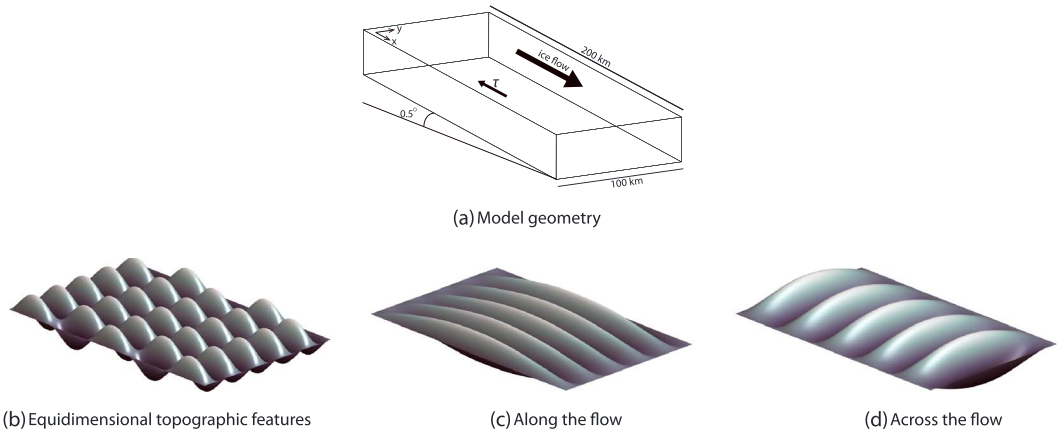

Figure 1. Model geometry and the shape of basal undulations.

To evaluate the influence of topography on ice and water flows, we consider three different topographic geometries: undulations with their long axes aligned with ice flow, undulations aligned perpendicular to flow, and equidimensional sinusoids with no preferred orientation.

2. Ice and Water Flow Models

2.1. Model Geometry

We consider an idealized ice stream 200 km long and 100 km wide inclined 0.5° downstream in the direction of ice flow (Figure 1a). These geometric parameters are of the same order of magnitude as the Siple Coast ice streams. A variety of bed topographies are generated using interfering sine functions.

$$b = b_0 \sin\left(\frac{n_x x\pi}{L_x}\right) \sin\left(\frac{n_y y\pi}{L_y}\right) \tag{1}$$

in which b_0 represents the maximum amplitude of features (50 m), n_x and n_y are uniquely specified for each experiment and determine the number of features to be created in the x and y directions, respectively, and L_x and L_y represent the x and y dimensions of the domain. The idealized basal undulations represent, in a simplified way, bed variability under Antarctic ice streams [*Fretwell et al.*, 2013].

We use a finite-element model of two-way coupled ice and water flow to investigate how bed topography influences the distribution of basal water beneath an ice stream with an uneven bed. The model is a thermo-mechanically coupled ice stream flow model modified from *Sergienko and Hulbe* [2011] and *Sergienko* [2014], as described here.

2.2. Ice Flow Model

Ice flow is simulated using vertically integrated momentum and mass balance equations [*MacAyeal*, 1989].

$$\begin{aligned}\frac{\partial}{\partial x}\left[2\nu H\left(2\frac{\partial u_i}{\partial x}+\frac{\partial v_i}{\partial y}\right)\right]+\frac{\partial}{\partial y}\left[\nu H\left(\frac{\partial u_i}{\partial y}+\frac{\partial v_i}{\partial x}\right)\right]-\tau_x=\rho_i g H\frac{\partial S}{\partial x}\\ \frac{\partial}{\partial y}\left[2\nu H\left(2\frac{\partial v_i}{\partial y}+\frac{\partial u_i}{\partial x}\right)\right]+\frac{\partial}{\partial x}\left[\nu H\left(\frac{\partial u_i}{\partial y}+\frac{\partial v_i}{\partial x}\right)\right]-\tau_y=\rho_i g H\frac{\partial S}{\partial y}\end{aligned} \tag{2}$$

where $\mathbf{v_i} = \{u_i, v_i\}$ is ice velocity, g is the acceleration due to gravity, ρ_i is the ice density, H is the ice thickness, and S is the ice surface elevation.

$$\tau \equiv \{\tau_x, \tau_y\} = -\beta \mathbf{v_i} \tag{3}$$

is basal traction, where β is the traction parameter defined below, equation (2.5), and ν is ice viscosity

$$\nu = \frac{B(\bar{T})}{2\left[\left(\frac{\partial u}{\partial x}\right)^2+\left(\frac{\partial v}{\partial y}\right)^2+\frac{1}{4}\left(\frac{\partial u}{\partial y}+\frac{\partial v}{\partial x}\right)^2+\frac{\partial u}{\partial x}\frac{\partial v}{\partial y}\right]^{\frac{n-1}{2n}}} \tag{4}$$

where $n = 3$ is the Glen's flow law exponent and $B(\bar{T})$ is temperature-dependent ice stiffness computed according to the widely used Arrhenius relationship

$$B(\bar{T}) = A(\bar{T})^{-\frac{1}{n}} = \left[a \exp\left(-\frac{Q}{RT_\star}\right)\right]^{-\frac{1}{n}} \tag{5}$$

where $A(\bar{T})$ is an Arrhenius parameter, $T_\star = \bar{T} + 273.15 + T_p$ is the pressure-corrected temperature, T_p is a correction for the pressure dependence of the ice melting point, $\bar{T}$ is the vertically integrated ice temperature, $Q = 6 \cdot 10^4$ J mol^{-1} is the activation energy for creep, $a = 3.61 \cdot 10^{-13}$ Pa^{-3} s is the flow rate factor, and $R = 8.31$ J mol^{-1} K^{-1} is the universal gas constant [e.g., *Bueler and Brown*, 2009]. A justification to use $\bar{T}$ instead of T is provided in *Sergienko* [2014] that also provides a governing equation for $\bar{T}$

$$\frac{\partial \bar{T}}{\partial t} + u\frac{\partial \bar{T}}{\partial x} + v\frac{\partial \bar{T}}{\partial y} = \frac{1}{H}\left[\dot{a}\left(T_s - \bar{T}\right) - \dot{b}\left(T_b - \bar{T}\right) - \kappa_i \left.\frac{\partial T}{\partial z}\right|_b\right] + \frac{W}{c_p \rho_i H}, \tag{6}$$

where $\dot{b}$ is basal melting/freezing (positive for melting) defined as (8); T_b is temperature at the ice base, taken to be equal to the pressure-melting point temperature; c_p is the heat capacity of ice; $W = \sigma'_{ij}\dot{\epsilon}_{ij}$ is the internal heating rate due to ice deformation; and σ'_{ij} and $\dot{\epsilon}_{ij}$ are components of the deviatoric stress tensor and the strain rate tensor, respectively. We use the following parameters: atmospheric temperature, $T_s = -18$°C, surface accumulation/ablation (positive for accumulation) $\dot{a} = 0.03$ m a^{-1}, and the temperature gradient, $T_z = -42$ mK m^{-1}, a typical observed value at the base of Siple Coast ice streams [*Engelhardt*, 2004].

The mass balance is

$$\frac{\partial H}{\partial t} = -\nabla \cdot \left(\mathbf{u_i} H\right) + \dot{a} - \dot{b} \tag{7}$$

where

$$\dot{b} = \frac{k_i T_z + G + \tau \cdot \mathbf{v_i}}{L\rho_i} \tag{8}$$

where $k_i = 2.2$ W m^{-1} K^{-1} is the thermal conductivity of ice, geothermal heat flux, $G = 65$ mW m^{-2}, and $L = 334$ kJ kg^{-1} is the latent heat of fusion.

2.3. Subglacial Water Flow Model

The basal water flow model follows *Clarke and Echelmeyer* [1996] and *Clarke* [2005]. Basal water is treated as a distributed system in which the flow is sheet like and velocity is proportional to the gradient in the hydraulic potential. Water depth is thus

$$\frac{\partial w}{\partial t} = -\nabla \cdot \left(\mathbf{u_w} w\right) + \dot{b} \tag{9}$$

in which w represents water depth and $\mathbf{u_w}$ represents the horizontal, depth-averaged water velocity. The water velocity $\mathbf{u_w}$ is

$$\mathbf{u_w} = -\frac{K}{\rho_w g}\nabla\phi \tag{10}$$

in which the material property K is the hydraulic conductivity of the water layer, ρ_w represents the density of the water, and ϕ represents the hydraulic potential field

$$\phi = p_w + \rho_w g b \tag{11}$$

which depends on water pressure p_w

$$p_w = \rho_i g H - N \tag{12}$$

and bed elevation b.

In a distributed system, the water pressure is approximately equal to the ice overburden pressure, in which case the effective pressure N is zero. This approximation is justified by observations of water pressures beneath the Ice Stream B which found the basal water pressure to be very close to the ice overburden pressure [*Engelhardt et al.*, 1990]. The effects of nonzero effective pressure are investigated in numerous studies [e.g., *Kyrke-Smith et al.*, 2013]. Using this simplification, the hydraulic potential gradient is thus

$$\nabla\phi = \rho_i g \nabla S + \left(\rho_w - \rho_i\right) g \nabla b \tag{13}$$

in which S represents the ice surface elevation and ρ_w represents the density of water. The well-known approximately 10:1 effect of ∇S and ∇b on water flow is clear [*Shreve*, 1972]. When two-way coupling is in effect, not only does ∇S drive water flow, but the resulting spatial variation in bed lubrication feeds back to S via gradients in the velocity field. We are interested in how ∇b mediates that feedback. Similar to previous studies [e.g., *Bougamont et al.*, 2011; *Bougamont and Christoffersen*, 2012], we disregard the effects of drainage in the subglacial hydraulic system. In contrast to studies focused on the long-term behavior (several thousand years), and assume that the subglacial hydraulic system is in a dynamic equilibrium with the overlying ice geometry, and disregard the evolution of water thickness, the $\frac{\partial w}{\partial t}$ term in equation (9) [e.g., *Goeller et al.*, 2013; *Bougamont et al.*, 2015], we do not make any assumptions of its behavior.

2.4. Boundary Conditions

Boundary conditions on the governing equations are the following: There is no ice flow through the lateral boundaries, i.e., $\mathbf{v_i} = 0$, and no-jump conditions are specified at the upstream and downstream boundaries for the vertically integrated forces in the x and y directions [*Sergienko et al.*, 2007]. The water depth, w, is set to 0 at all boundaries apart from the downstream one. The ice stream thickness is set initially to a uniform value of 1 km. At the upstream end the thickness is held fixed at 1 km. A zero flux boundary condition is applied along all other margins. The boundary conditions for $\bar{T}$ are similar to the ice thickness boundary conditions: the temperature is prescribed at the upstream end ($\bar{T} = -15°\mathrm{C}$), and the zero flux boundary condition is prescribed at all other boundaries.

2.5. Numerical Implementations

Many models account for the flow of ice and of water, but without two-way coupling [*Le Brocq et al.*, 2009; *Sergienko and Hulbe*, 2011]. Feedbacks that may alter the ice thickness, water depth, and flow of both materials are missing. Changes in the geometry will affect the flow of water by altering the gradients in the hydraulic potential and could redistribute the water in such a way as to reinforce or halt further changes in ice geometry. *Sergienko and Hulbe*'s [2011] treatment of basal traction is modified so that ice and water flow are coupled together. The traction parameter β is defined as

$$\beta(w) = \begin{cases} \beta_c \left(1 - \frac{w}{w_c}\right) & \text{if } w < w_c \\ 0 & \text{if } w \geq w_c \end{cases} \tag{14}$$

where β_c is a constant and w_c is the critical water depth at which the basal traction becomes zero (chosen to be 0.5 m in this study). As the water layer depth approaches w_c, the basal traction reduces to zero. In order to avoid abrupt transitions in β as $w \rightarrow w_c$, we smooth over the length of several nodes. The choice of the w_c value is arbitrary. Its magnitude affects the timescales of the processes described below but does not change their nature.

All simulations are done using a finite-element solver, COMSOL™. All equations are solved simultaneously at each time step using a modified form of the damped Newton iteration method paired with a direct solver Multifrontal Massively Parallel Sparse direct Solver to solve a linearized system of equations (COMSOL™ User Guide). At each time step, the solution (computed variables) satisfies all equations simultaneously within a convergence tolerance (10^{-6}). We use triangular elements with linear dimensions ~600 m in the domain and rectangular elements (~40 m) in boundary layers near the lateral boundaries in order to properly simulate no flow conditions at these boundaries.

2.6. Initialization

The model is initialized in a two-step process, beginning with the ice velocity, thickness, and temperature and then moving on to couple these with the water flow model. Coupling proceeds in two steps, first, one way, between an initial water field and the overlying ice, and then finally, the full two-way coupling is enacted. Since ice and water respond to perturbations at different timescales, this sequence ensures that the model converges at the final step.

Initialization begins by iteratively solving the ice flow equations with the specified boundary conditions and parameters to produce initial, steady state ice velocity, thickness, and temperature fields. The water depth is then initialized to a field that is a steady state response to the previously determined ice thickness and velocity.

At this stage we have an uncoupled, steady state solution to the system of equations. It should be noted that the two solutions are not necessarily internally consistent. Model coupling proceeds as follows:

1. One-way coupling — in which the ice responds to the initial basal water depth field — is achieved by updating the basal traction parameter and obtaining updated ice thickness and velocity fields. This step ensures internal consistency between the ice thickness, ice velocity, and water depth fields.
2. Two-way coupling proceeds by solving the ice and water flow equations in a transient simulation — using the results of the prior steps as initial conditions — and allowing the water flow to respond to changes in the ice flow.

In a few experiments, numerical instabilities produce unreasonable water depths. Such instabilities are known to appear in numerical models of thin film flows [e.g., *Le Brocq et al.*, 2009]. Here they arise at isolated nodes and our remedy is to set a maximum water depth of 20 m, above which spiked values are reset to the maximum. The procedure affects very few nodes in the experiments where it is applied.

2.7. Model Limitations

As is apparent in their description, the ice and subglacial water flow models used here disregard some physical process that, if important, would modify their interaction. The linear sliding law equation (3) does not account for richness of behaviors produced with multivalued sliding laws [e.g., *Kyrke-Smith et al.*, 2013; *Kyrke-Smith and Fowler*, 2014; *Schmittner and Tziperman*, 2009; *Zoet and Iverson*, 2015]. The subglacial flow model explicitly assumes that the effective pressure $N = 0$. This eliminates the possibility of oscillations in subglacial water pressure and the resulting effects on ice flow, e.g., seasonal ice flow speedup observed on Greenland outlet glaciers and mountain glaciers due to input of meltwater [e.g., *Hewitt*, 2012; *Schoof et al.*, 2014; *Kingslake*, 2015]. Also, the model excludes the effect of sediment transport [e.g., *Creyts and Schoff*, 2009; *Kyrke-Smith and Fowler*, 2014], which may cause basal morphology to change over time. We justify these choices and discuss their effects in section 4.

3. Model Experiments

The two-way coupled model is used to examine the influence of three types of geometries on the storage and transport of basal water. The idealized basal features differ in their along and across flow aspect ratios and are analogues to three glacial geomorphic features:

1. Interfering equidimensional sinusoids might be envisioned to represent a rough bed dominated by obstacles at a particular spatial scale (Figure 1b).
2. Undulations with their long axes aligned parallel to ice flow might be envisioned as flutes or mesoscale liniations (Figure 1c).
3. Undulations with their long axes aligned perpendicular to ice flow might be envisioned as reflecting a bedrock jointing pattern or rogen moraines (Figure 1d).

The three types of geometries produce distinctive spatial and temporal characteristics in the distribution of basal water and the overlying ice.

Fundamental patterns and their differences are illustrated using representative outputs from larger suites of model runs. Figures show time-averaged characteristics of ice stream flow (ice speed, thickness, basal shear, and effective stress, τ_{eff}, defined as $2\tau_{\text{eff}}^2 = \sigma'_{ij}\sigma'_{ij}$) and subglacial water flow (subglacial water depth and its speed). The temporal evolution is illustrated by movies in the supporting information. Year-to-year spatial variability is demonstrated using two snapshots of the subglacial water depth and the deviation of ice stream flow characteristics from their time-averaged values. These examples are presented for the topography with undulations oriented across ice stream flow (Figures 5 and 6). The magnitudes and spatial distributions of these two snapshots are not the same for similar fields obtained in simulations with other topographic shapes, and they are also not the same for different snapshots from the same simulation. Nevertheless, they illustrate variability in the ice stream/subglacial hydraulic system simulated in this study.

Following the initialization procedure, the two-way coupled model was run for 50 years at 30 day time steps. In order to test the effects of the initialization procedure on the obtained results, we have performed the same set of simulations with the initial water depth, w, set to zero. While spatial patterns of the water depth distribution are not exactly the same in the two cases, the temporal patterns are very similar; i.e., characteristic timescales are the same as described below. Movie S7 illustrates the behavior of the subglacial water depth in this simulation.

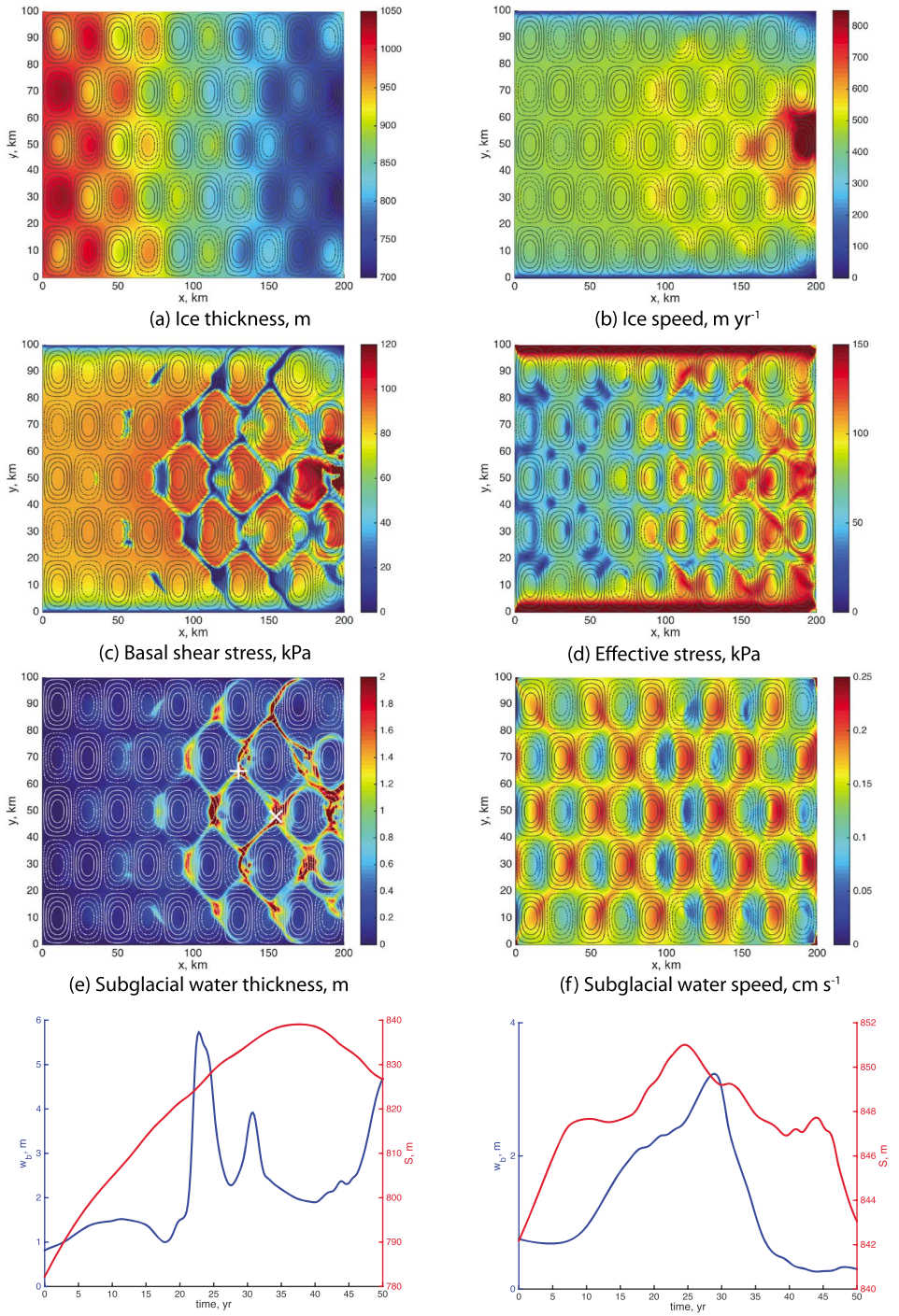

Figure 2. Hummocky topography. Time-averaged (a) ice thickness, m; (b) ice speed, m yr^{-1}; (c) basal shear stress, kPa; (d) effective stress, kPa; (e) subglacial water thickness, m; and (f) subglacial water speed, cm s^{-1}. Contours indicate bed topography, solid lines are positive values, and dashed lines are negative values. (g and h) Time series of subglacial water depth, m (blue curve, left vertical axis), and ice thickness rate of change, $year^{-1}$ (red curve, right vertical axis), at points indicated by cross and plus symbols in Figure 2e.

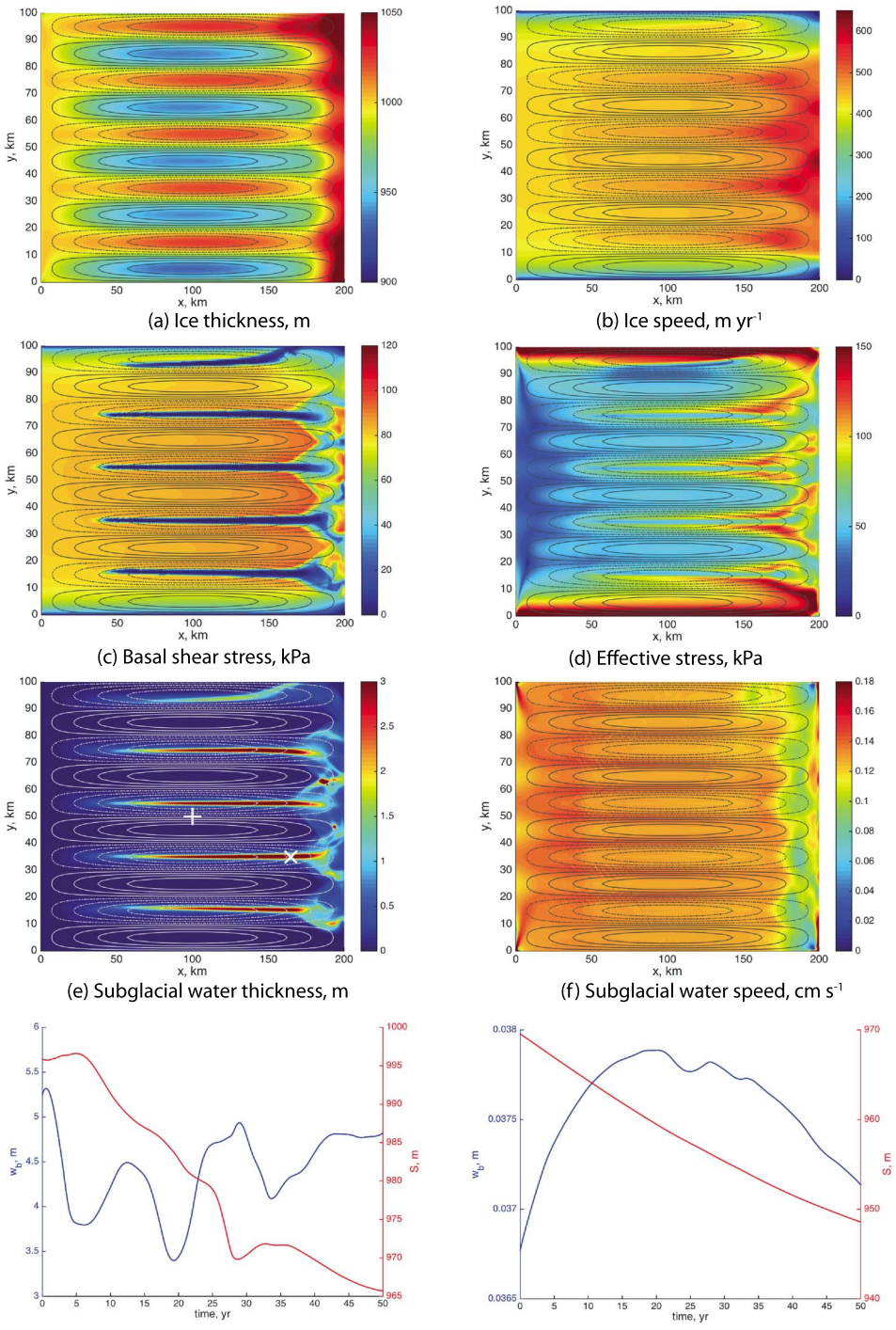

Figure 3. Along flow topography. Panels are the same as in Figure 2.

3.1. Hummocky, Equidimensional Topography

The coupled ice stream and subglacial water flows over a "hummocky" bed of equidimensional sinusoids ($n_x = 10$ and $n_y = 5$) (Figure 1b) yield a system of interconnected, locally deep water layers (ponds) that develop close to the topographic lows (Figure 2e). This water spills around the flanks of the hills toward other ponds through channel-like features (~3 km wide) oriented obliquely to the direction of ice flow. The locations of the ponds and channels are predominantly controlled by the basal undulations: they tend to form between neighboring topographic lows and occasionally between topographic lows and highs (Movie S1).

The subglacial flow exhibits temporal variability on timescales of a few years to a decade (Movie S1). The changes in basal traction β, and hence in basal shear τ, are due to the presence of subglacial water and result in speedup (β reduces) or slowdown (β increases) of ice flow (Figure 2c). This consequently leads to changes in ice thickness and surface elevation, which, in turn, affect subglacial water flow. Figures 2g and 2h show evolution of subglacial water depth (blue curve, left vertical axes) and ice surface elevation (red curve, right vertical axes) at two points near subglacial ponds (cross and plus symbols in Figure 2e). Though water depth and ice surface elevation exhibit strong temporal variability, they do not covary. This emphasizes the strong nonlocality of ice stream flow. The geometric and kinematic characteristics of ice stream flow at a given location are results of the cumulative effects of temporal variations in basal conditions that take place at locations as far as tens of kilometers away [e.g., *Sergienko et al.*, 2007].

The feedback between basal traction and subglacial water (equation (14)) results in the spatial variability of basal shear and, consequently, ice stream flow (Figures 2b and 2c), which leads to variability in strain rates and consequently to spatial (Figure 2d) and temporal (Movie S2) variability of the effective stress. The relatively large magnitudes of the effective stress (~150–200 kPa) indicate that surface crevasses might form in locations where such high effective stresses are achieved. The complex temporal and spatial patterns of the effective stress (Movie S2) suggest that crevasses might not be simply advected with ice stream flow but may also undergo structural evolution due to the effects of variability in the subglacial water system.

3.2. Topographic Features Oriented Along Flow

We consider basal undulations with five wave cycles ($n_y = 10$) that together make a set of four parallel subglacial troughs (the fifth is at the edge of the model domain, Figure 1c). The troughs deepen and shallow with distance downstream ($n_x = 1$). Basal troughs create local potential lows that collect and guide water downstream (Figures 3e and 3f). The shallowing of the troughs near the downstream end of the domain allows for lateral spreading of subglacial water, with formation of fanned branches or channel-like features (Movie S3) similar to those observed in simulations with hummocky topography described above. Less constricted by the ridges in the downstream end, these features interact with each other allowing for converging and diverging spatial patterns. The temporal evolution of subglacial water depth at a point inside a trough (cross symbol in Figure 3e) has multidecadal variability (blue curve, left vertical axes, and the rate of ice thickness change, red curve, right vertical axes, Figure 3g). However, the fanned tunnel-like features exhibit variability on shorter timescales, ~3–7 years (Movie S3). In contrast, water depth on subglacial crests has almost no variability (plus symbol in Figure 3e), though the surface experiences long-term lowering as the overall geometry of the stream changes (Figure 3h).

As in the case of hummocky topography, the simulated spatial and temporal variability in ice flow is associated with variability in ice stresses (Figures 3b–3d and Movie S4). In this case, effective stresses are enhanced close to the undulation ridges. However, unlike the hummocky case, the effect is concentrated near those features, rather than distributed over a large area of the model domain. The bands of relatively high effective stress are less oblique to ice flow than in the hummocky case (Movies S4 and S2). The elongated spatial patterns with high effective stress are less oblique to the direction of ice flow compared to similar patterns in the hummocky bed simulations (Movies S4 and S2).

3.3. Topographic Features Oriented Transverse to Flow

The most dynamic of our basal water systems are produced in simulations with basal topographic undulations with long axes oriented transverse to ice flow (Figures 4e and 4f and Movie S5). As in the other simulations, channel-like spatial patterns emerge but the channels exhibit temporal variability on shorter timescales (~2–4 years). The channels tend to be oriented obliquely to the direction of ice flow, but with smaller angles than in the hummocky bed case (Movies S5 and S1). Subglacial ponds also form; however, they are less stable than in the other cases and drain and reform in different locations (Movie S5). The temporal variability of the subglacial water depth and surface elevation (blue curve, left vertical axes, and red curve, right vertical axes,

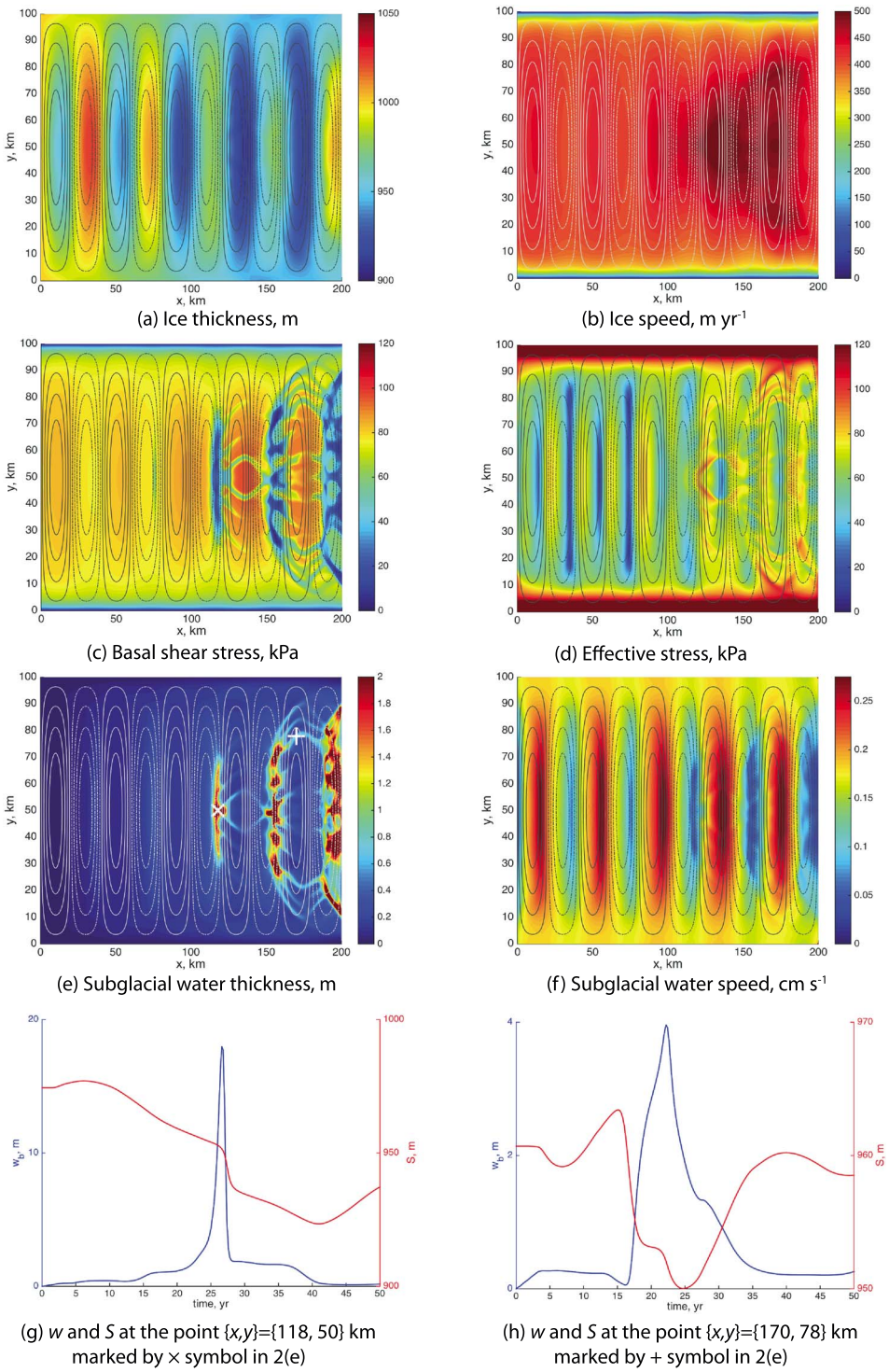

Figure 4. Along flow topography. Panels are the same as in Figure 2.

respectively, Figures 4g and 4h) at two points where subglacial water ponds (cross and plus symbols in Figure 4e) have complicated structures shows rapid formation and drainage (~5 years at a point marked with cross) followed by a slow inflation and deflation on much longer (approximately decadal) timescales. The corresponding ice thickness and surface elevation changes occur on much shorter timescales.

Similar to simulations with the hummocky bed topography, coupling with subglacial water flow on a bed with transverse undulations affects a large area of the ice stream flow (Figure 4b). Consequent variability in

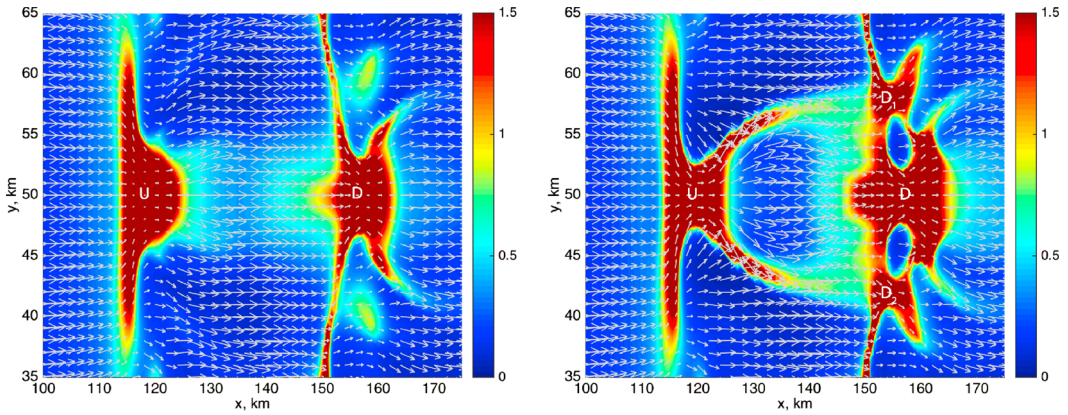

Figure 5. Snapshots of subglacial water thickness (m) (color) and velocity (arrows) before and after a lake drainage event.

the effective stress has complex temporal and spatial patterns (Figure 4d and Movie S6). Where channel-like subglacial water structures are present, localized speedup of ice flow causes narrow, elongated patterns of high effective stress. The bed with transverse undulations gives rise to a larger concentration of such patterns than the other bed morphologies. The prevailing orientation of these high effective stress zones is oblique to ice flow.

3.4. Snapshots of the Ice Stream/Subglacial Water System States

The simulated ice stream/subglacial water systems exhibit high temporal variability in all experiments, as Movies S1–S6 illustrate. Although the time-averaged fields (Figures 2–4) reflect the general, ice stream wide, spatial patterns adequately, the averaging procedure eliminates smaller-scale variability, resulting in a relatively smooth appearance. In addition, the magnitudes of the time-averaged fields have significantly lower maximum and minimum values than the magnitudes of the instantaneous fields. In order to demonstrate

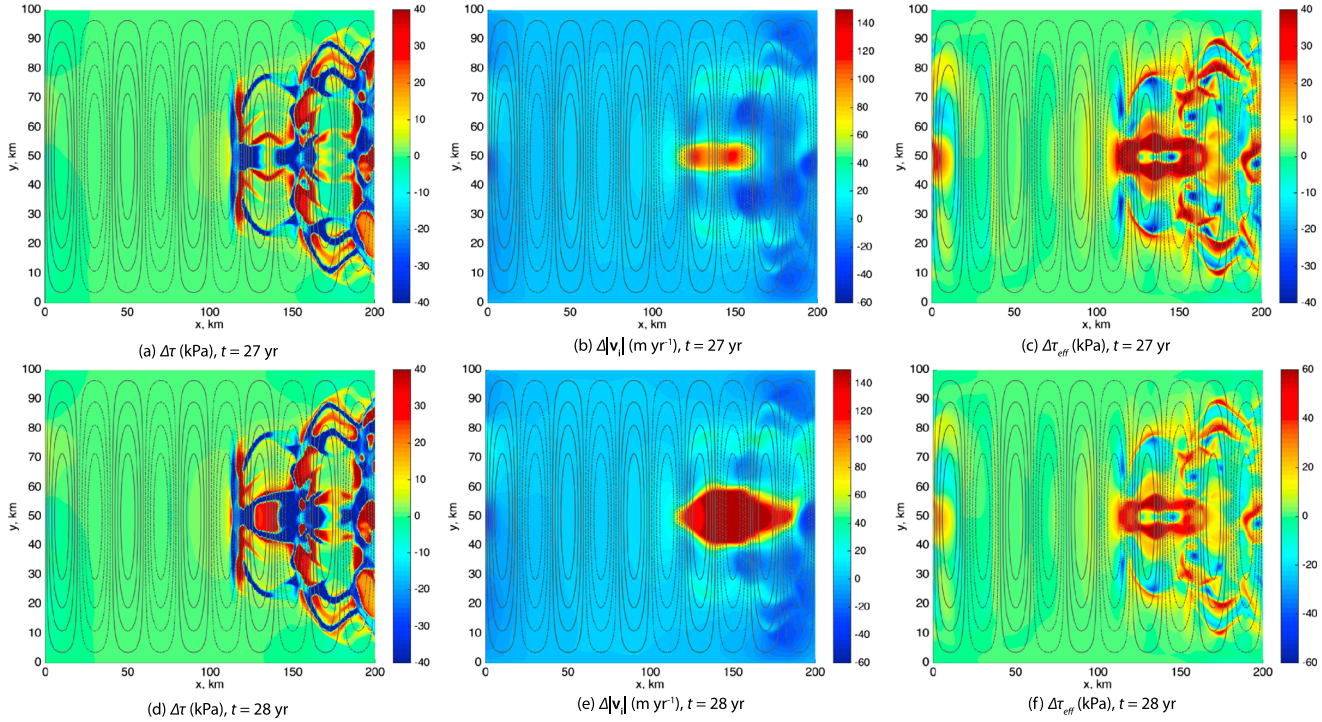

Figure 6. Deviations of basal shear, τ, ice speed, $|\mathbf{v_i}|$, and effective stress, τ_{eff}, from time-averaged fields shown in Figure 4 at $t = 27$ years and $t = 28$ years. Note the different color scales in Figures 6c and 6f.

a fuller range of variability in the coupled model, we examine instantaneous states at two points in time, $t = 27$ years and $t = 28$ years in the simulation with topographic undulations oriented across ice stream flow. The overall behavior, i.e., larger range of instantaneous magnitudes compared to the time-averaged magnitudes and the small-scale heterogeneity, is representative of the ice stream/subglacial hydraulic system states simulated in this study.

Over the interval between the two snapshots, one of the pond-like features (U in Figure 5) partially drains toward a downstream pond (D in Figure 5) and two new ponds (D1 and D2) begin to form, on either side of the existing downstream lake. The drainage occurs through two channel-like features that act as pathways to transport water from the upstream lake U to the downstream lakes D1 and D2. Prior to the drainage event, basal shear stress τ is zero over the areas occupied by the lakes U and D (Figure 6a). In other areas, where the snapshot subglacial water thickness is smaller than the time-averaged thickness, basal shear stress is relatively high. This distribution of basal shear results in faster ice flow over the two ponds, relative to the time-averaged speed (Figure 6b), and slower flow in other locations. The corresponding instantaneous effective stress (Figure 6c) is larger than the time-averaged values over areas characterized by a sharp transition in the basal shear stress. Drainage of pond U (Figure 5) alters the basal shear distribution and causes the ice to flow faster than it did prior to the event (Figure 6e). The snapshot ice speed is more than 30% larger than the time-averaged value (Figure 4b), and the effective stresses resulting from the speedup are more than 50% larger than the time-averaged values (Figures 6e and 6f).

4. Discussion

We simulate ice stream flow over three types of undulated bed morphologies—hummocky (equidimensional), elongated along flow, and elongated transverse to flow—using a two-way coupled ice stream/subglacial water flow model. Dynamic subglacial water systems develop in ways that depend on both the length scale and orientation of undulations with respect to the ice stream flow. All three types of undulations support narrow channel-like features in subglacial water flow that are oriented obliquely to ice flow. The oblique channels, in some cases accompanied by ponds, vary on multiyear to decadal timescales as a result of feedbacks between subglacial water and ice flow. In the hummocky case, the location and size of subglacial water features appears to be predominantly constrained by the topography.

In our model, feedbacks between water and ice operate as follows. As the subglacial water thickness increases either due to in situ basal melting or due to inflow from upstream, the basal traction reduces locally. This causes a localized speedup of ice flow, which in turn causes ice thinning and changes the surface slope [*Sergienko et al.*, 2007]. The latter changes the hydraulic potential that controls subglacial water flow and its distribution. The specifics of water distribution depend on the characteristics of the topographic undulations. In particular, subglacial water ponding is observed in simulations with hummocky and transverse undulations. In the hummocky case, subglacial ponds remain spatially fixed with respect to the topographic lows. In the transverse undulations case, ponds are not tied to the topographic lows and they form, drain through the channel-like features, and reform in different locations. Additionally, subglacial water affects basal melt. Where water depth exceeds the critical water depth, w_c, basal melting is substantially reduced because basal shear τ is zero (equation (8)). The variability in basal melting affects ice temperature (equation (6)) and, as a result, its viscosity (equation (5)).

The channel-like subglacial features form spontaneously due to the feedbacks described above. The obliquity of the pathway orientation relative to ice flow changes depending on the topography. In simulations where the topographic features are oriented parallel to ice flow, the obliquities have the smallest angles (i.e., closer to the direction if ice flow). The obliquity is larger in simulations with hummocky undulations. The characteristic width of the channel-like features is ~2–4 km, which is well resolved in our simulations with mesh resolution 600 m or less. The temporal scales on which the channel configurations change are also controlled by bed morphology. The fastest variability occurs in the transverse undulation case (~2–4 years), and the slowest occurs in the hummocky case.

The channel-like features that form in our simulations have transverse dimensions at least 2 orders of magnitude larger than the subglacial channels or conduits (~10–50 m) observed on mountain glaciers. Those features are melted by turbulent water flow, and their size is determined by the balance between melting and creep closure [e.g., *Nye*, 1976]. The key difference between the channel-like features simulated in our study

and these narrow conduits is nonzero effective pressure, the gradient in which is a highly nonlinear function of the water flux and the conduit cross section [e.g., *Fowler*, 1999; *Hewitt*, 2011]. In the absence of any interaction with ice flow, this nonlinear dependence and an assumption of turbulent flow in the conduit gives rise to oscillatory [e.g., *Fowler*, 1999; *Schoof et al.*, 2014] and chaotic behaviors [e.g., *Kingslake*, 2015]. In contrast, in our simulations, the subglacial water flow is laminar (the characteristic Reynolds numbers are $Re \lesssim 10$), and the channel-like features cannot be formed without interactions between subglacial water and ice flow. They are a direct result of the feedbacks among basal traction affected by the subglacial water distribution, ice stream flow, and geometry that affect hydraulic potential and hence subglacial water flow.

It is tempting to speculate that such highly variable channel-like structures relate to formation of rib-like patterns of high basal shear inferred using inverse methods under large areas of Antarctica and Greenland. Like the water features simulated here, those patterns are oriented obliquely to the direction of ice flow [*Sergienko and Hindmarsh*, 2013; *Sergienko et al.*, 2014]. The proposed mechanisms for rib-like patterns include dynamic subglacial water and sediment systems [*Sergienko and Hindmarsh*, 2013]. Although we do not simulate sediment transport in this study, the development of the oblique channel-like subglacial water structures may promote formation of subglacial sediment structures oriented in the same direction. These structures also resemble drainage networks observed in benchtop experiments carried out by *Catania and Paola* [2001]. They conducted laboratory experiments demonstrating that pressurized water flow over a noncohesive bed will produce a braided channel system controlled by variations in the lateral pressure gradients. Although the water flow in the model experiments is gravity driven and no substrate is considered, the model results bear strong resemblance to those experimental results.

Spatial and temporal variability in the interaction between ice and subglacial water flow has strong effects on the ice stream stress distributions. Ice flow over areas where basal traction experiences strong gradients results in large effective stresses that could cause crevasse formation. They could explain the anomalous strain rate patterns reported on by *Hulbe and Whillans* [1997]. As the locations of the large basal traction gradients migrate with time, the spatial patterns with high effective stress migrate as well. These patterns are not only advected with ice flow but also undergo internal (ice stream/subglacial water system) evolution. The orientation of elongated patterns of high effective stress is oblique to ice flow as well. We suggest that obliquely oriented surface crevasses observed on ice streams outside of the shear margins where patterns are stationary might be caused by the presence of dynamic subglacial systems underneath them.

As our analysis shows, the instantaneous characteristics of the ice stream/subglacial water system have magnitudes substantially different from their time-averaged values. This suggests that short-term events like drainage of a subglacial lake can result in high-amplitude instantaneous response (Figure 6e), which is less pronounced in the time-averaged quantities. Instantaneous observations of ice streams and especially subglacial water system may not reflect their long-term behavior. The temporal variability of the subglacial water system is highly heterogeneous. For instance, subglacial water depth remains almost constant at some locations (Figure 3h). This suggests that fairly sparse observations of ice stream surface changes do not reflect the variability of basal conditions and potentially of the subglacial hydraulic system on large spatial scales. Significantly higher spatial resolution than, for example, satellite tracks [e.g., *Fricker et al.*, 2007; *Smith et al.*, 2009] are required to assess the behavior of subglacial hydraulic systems.

We point out that the ice stream/subglacial water systems simulated in this study do not show signs of attaining steady state configurations. The feedbacks between subglacial water thickness and the basal traction coefficient yield ongoing temporal variability of the systems. Although our simulations are highly idealized and extension of their results to real ice streams is perhaps overreaching, it nevertheless may be possible that the notion of ice streams steady states is artificial, and as observations show, they are neither in steady state currently nor may achieve such states in the future nor had in the past. Instead, a question about scales of their temporal variability may be more relevant. Recent observations suggest that short-term (several years) variability of ice flow is common on a number of Siple Coast ice streams [eg., *Hulbe et al.*, 2016].

It is important to note that the coupling between subglacial water flow and basal traction used in this study is heuristic. However, the chosen formulation reflects the observed relationship between decreases in traction with the increase in subglacial water layer depth. Most likely, timescales of the formation and evolution of subglacial water features (e.g., channel-like structures and ponds) are affected by the arbitrary chosen form and parameters of our basal traction formulation (equation (14)), as well as other poorly constrained parameters (e.g., the hydraulic conductivity). In the absence of the direct observations of such parameters and

temporal evolution of subglacial system that can provide constraints on the ice stream basal conditions, the formulations of feedbacks between basal traction and subglacial water system remain uncertain.

5. Conclusions

Our study demonstrates that ice stream flow over spatially heterogeneous topography with even simple dependence of basal traction on subglacial water parameters (e.g., depth) results in the development of a complex subglacial water system. The feedbacks between basal traction, ice flow, and surface slopes result in the development of spatially and temporally variable subglacial water distributions. The orientation and wavelength of topographic undulations determine the timescales, nature (e.g., the presence of pond- or channel-like features), and orientation of the subglacial water structures. The variability of the simulated coupled ice stream/subglacial water system on short timescale (several years to decades) suggests that the observed short-term surface variations can be indicative of a rapidly evolving subglacial system. Further progress in the understanding of this coupled ice stream/subglacial water system requires direct observations of subglacial conditions.

Acknowledgments
We thank the Associate Editor, Poul Christoffersen, Jonny Kingslake, and two anonymous referees for their useful suggestions and constructive criticism that helped to improve the manuscript. This study is supported by U.S. National Science Foundation grant OPP-0838811 and by NOAA grant NA13OAR431009. The model outputs will be available at NSIDC nsidc.org.

References

Bougamont, M., and P. Christoffersen (2012), Hydrologic forcing of ice stream flow promotes rapid transport of sediment in basal ice, *Geology*, *40*, 735–738, doi:10.1130/G33036.1.
Bougamont, M., S. Price, P. Christoffersen, and A. J. Payne (2011), Dynamic patterns of ice stream flow in a 3-D higher-order ice sheet model with plastic bed and simplified hydrology, *J. Geophys. Res.*, *116*, F04018, doi:10.1029/2011JF002025.
Bougamont, M., P. Christoffersen, S. F. Price, H. A. Fricker, S. Tulaczyk, and S. P. Carter (2015), Reactivation of Kamb Ice Stream tributaries triggers century-scale reorganization of Siple Coast ice flow in West Antarctica, *Geophys. Res. Lett.*, *42*, 8471–8480, doi:10.1002/2015GL065782.
Bueler, E., and J. Brown (2009), Shallow shelf approximation as a "sliding law" in a thermomechanically coupled ice sheet model, *J. Geophys. Res.*, *114*, F03008, doi:10.1029/2008JF001179.
Carter, S., D. Blankenship, M. Peters, D. A. Young, J. W. Holt, and D. L. Morse (2007), Radar-based subglacial lake classification in Antarctica, *Geochem. Geophys. Geosyst.*, *8*, Q03016, doi:10.1029/2006GC001408.
Carter, S., D. Blankenship, D. Young, M. Peters, J. Holt, and M. Siegert (2009), Dynamic distributed drainage implied by the flow evolution of the 1996–1998 adventure trench subglacial lake discharge, *Earth Planet. Sci. Lett.*, *283*, 24–37.
Carter, S., H. Fricker, D. Blankenship, J. Johnson, W. Lipscomb, S. Price, and D. Young (2011), Modeling 5 years of subglacial lake activity in the MacAyeal Ice Stream (Antarctica) catchment through assimilation of ICESat laser altimetry, *J. Glaciol.*, *57*(206), 1098–1112.
Catania, G., and C. Paola (2001), Braiding under glass, *Geology*, *29*(3), 259–262.
Clarke, G. (2005), Subglacial processes, *Annu. Rev. Earth. Planet. Sci.*, *33*, 247–276.
Clarke, T., and K. Echelmeyer (1996), Seismic-reflection evidence for a deep subglacial trough beneath Jakobshavn Isbræ, West Greenland, *J. Glaciol.*, *141*(42), 219–232.
Creyts, T., and C. Schoff (2009), Drainage through subglacial water sheets, *J. Geophys. Res.*, *114*, F04008, doi:10.1029/2008JF001215.
Engelhardt, H. (2004), Thermal regime and dynamics of the West Antarctic ice sheet, *Ann. Glaciol.*, *39*, 85–92.
Engelhardt, H., N. Humphrey, B. Kamb, and M. Fehnestock (1990), Physical conditions at the base of a fast moving Antarctic ice stream, *Science*, *248*, 57–59.
Fowler, A. (1999), Breaking the seal at Grímsvötn, Iceland, *J. Glaciol.*, *45*(151), 506–516.
Fretwell, P., et al. (2013), Bedmap2: Improved ice bed, surface and thickness datasets for Antarctica, *Cryosphere*, *7*, 375–393, doi:10.5194/tc-7-375-2013.
Fricker, H., and T. Scambos (2009), Connected subglacial lake activity on lower Mercer and Whillans ice streams, West Antarctica, *J. Glaciol.*, *55*(190), 303–315.
Fricker, H., T. Scambos, R. Bindschadler, and L. Padman (2007), An active subglacial water system in West Antarctica mapped from space, *Science*, *315*(5818), 1544–1548.
Fried, M., C. Hulbe, and M. Fahnestock (2014), Grounding-line dynamics and margin lakes, *Ann. Glaciol.*, *55*(66), 87–96.
Goeller, S., M. Thoma, K. Grosfeld, and H. Miller (2013), A balanced water layer concept for subglacial hydrology in large-scale ice sheet models, *Cryosphere*, *7*(4), 1095–1106, doi:10.5194/tc-7-1095-2013.
Gray, L., I. Joughin, S. Tulaczyk, V. Spikes, R. Bindschadler, and K. Jezek (2005), Evidence for subglacial water transport in the West Antarctic Ice Sheet through three-dimensional satellite radar interferometry, *Geophys. Res. Lett.*, *32*, L03501, doi:10.1029/2004GL021387.
Gudmundsson, G. (2003), Transmission of basal variability to a glacier surface, *J. Geophys. Res.*, *108*(B5), 2253, doi:10.1029/2002JB002107.
Hewitt, I. J. (2011), Modelling distributed and channelized subglacial drainage: The spacing of channels, *J. Glaciol.*, *57*(202), 302–314.
Hewitt, I. J. (2012), Seasonal changes in ice sheet motion due to melt water lubrication, *Earth Planet. Sci. Lett.*, *371–372*, 16–25.
Hulbe, C., and I. Whillans (1997), Weak bands within Ice Stream B, West Antarctica, *J. Glaciol.*, *43*(145), 254–262.
Hulbe, C. L., T. A. Scambos, M. Klinger, and M. A. Fahnestock (2016), Flow variability and ongoing margin shifts on Bindschadler and MacAyeal Ice Streams, West Antarctica, *J. Geophys. Res. Earth Surf.*, *121*, doi:10.1002/2015JF003670.
Kingslake, J. (2015), Chaotic dynamics of a glaciohydraulic model, *J. Glaciol.*, *61*(227), 493–502, doi:10.3189/2015JoG14J208.
Kyrke-Smith, T. M., and A. Fowler (2014), Subglacial swamps, *Proc. R. Soc. A*, *470*, 20140340, doi:10.1098/rspa.2014.0340.
Kyrke-Smith, T. M., R. Katz, and A. Fowler (2013), Subglacial hydrology and the formation of ice streams, *Proc. R. Soc. A*, *470*, 20130494, doi:10.1098/rspa.2013.0494.
Le Brocq, A., A. J. Payne, M. Siegert, and R. Alley (2009), A subglacial water-flow model for West Antarctica, *J. Glaciol.*, *55*(193), 879–888.
MacAyeal, D. (1989), Large-scale ice flow over a viscous basal sediment: Theory and application to ice stream B, Antarctica, *J. Geophys. Res.*, *94*(B4), 4071–4087.
Nye, J. F. (1976), Water flow in glaciers: Jökulhlaups, tunnels and veins, *J. Glaciol.*, *17*(76), 181–207.

Schmittner, A., and E. Tziperman (2009), Spatiotemporal dynamics of ice streams due to a triple-valued sliding law, *J. Fluid Mech.*, *640*, 483–505.
Schoof, C. (2002), Basal perturbations under ice streams: Form drag and surface expression, *J. Glaciol.*, *48*(162), 407–416.
Schoof, C., C. A. Rada, N. J. Wilson, G. E. Flowers, and M. Haseloff (2014), Oscillatory subglacial drainage in the absence of surface melt, *Cryosphere*, *8*(3), 959–976, doi:10.5194/tc-8-959-2014.
Sergienko, O. (2012), The effects of transverse bed topography variations in ice-flow models, *J. Geophys. Res.*, *117*, F03011, doi:10.1029/2011JF002203.
Sergienko, O. (2013), Glaciological twins: Basally controlled subglacial and supraglacial lakes, *J. Glaciol.*, *59*(213), 3–8, doi:10.3189/2013JoG12J040.
Sergienko, O., and R. C. A. Hindmarsh (2013), Regular patters in frictional resistance of ice-stream beds seen by surface data inversion, *Science*, *342*, 1086–1089.
Sergienko, O., and C. Hulbe (2011), "Sticky spots" and subglacial lakes under ice streams of the Siple Coast, Antarctica, *Ann. Glaciol.*, *52*(58), 18–22.
Sergienko, O., D. MacAyeal, and R. Bindschadler (2007), Causes of sudden, short-term changes in ice-stream surface elevation, *Geophys. Res. Lett.*, *34*, L22503, doi:10.1029/2007GL031775.
Sergienko, O. V. (2014), A vertically integrated treatment of ice stream and ice shelf thermodynamics, *J. Geophys. Res. Earth Surf.*, *119*, 745–757, doi:10.1002/2013JF002908.
Sergienko, O. V., T. T. Creyts, and R. C. A. Hindmarsh (2014), Similarity of organized patterns in driving and basal stresses of Antarctic and Greenland ice sheets beneath extensive areas of basal sliding, *Geophys. Res. Lett.*, *41*, 3925–3932, doi:10.1002/2014GL059976.
Shreve, R. (1972), Movement of water in glaciers, *J. Glaciol.*, *11*(62), 205–214.
Siegert, M., and J. Bamber (2000), Subglacial water at the heads of Antarctic ice-stream tributaries, *J. Glaciol.*, *46*(155), 702–703.
Smith, B., H. Fricker, I. Joughin, and S. Tulaczyk (2009), An inventory of active subglacial lakes in Antarctica detected by ICESat (2003–2008), *J. Glaciol.*, *55*(192), 573–595.
Tulaczyk, S., R. Pettersson, N. Quintana Krupinski, H. Fricker, I. Joughin, and B. Smith (2008), Do dynamic subglacial lakes impact temporal behavior of fast-flowing ice streams? GPS and radar investigations on two West Antarctic ice streams, *Geophys. Res. Abstr.*, *10*(11565), 1607–7962.
Wingham, D., M. Siegert, A. Shepherd, and A. Muir (2006), Rapid discharge connects Antarctic subglacial lakes, *Nature*, *440*, 1033–1036.
Zoet, L., and N. Iverson (2015), Experimental determination of a double-valued drag relationship for glacier sliding, *J. Glaciol.*, *61*(225), 1–7, doi:10.3189/2015JoG14J174.